ELSEVIER

Contents lists available at ScienceDirect

Composites Part B

journal homepage: www.elsevier.com/locate/compositesb





Characterizing friction for fiber reinforced composites manufacturing: Method development and effect of process parameters

Arit Das a,b , Gabriel Y.H. Choong c , David A. Dillard b,d , Davide S.A. De Focatiis c,** , Michael J. Bortner a,b,*

- ^a Department of Chemical Engineering, Virginia Tech, Blacksburg, VA, 24061, USA
- ^b Macromolecules Innovation Institute, Virginia Tech, Blacksburg, VA, 24061, USA
- E Department of Mechanical, Materials and Manufacturing Engineering, University of Nottingham, Nottingham, NG7 2RD, UK
- ^d Department of Biomedical Engineering and Mechanics, Virginia Tech, Blacksburg, VA, 24061, USA

ARTICLE INFO

Keywords: Carbon fiber Prepreg Rheological properties Optical microscopy Friction

ABSTRACT

In automated layup manufacturing processes of fiber-reinforced polymer composites, the quality of the manufactured part is strongly dependent on frictional behavior. Improper control of frictional forces can lead to defect formation. Frictional sliding rheometry tests provide an innovative methodology to accurately characterize the tool-ply friction of unidirectional (UD) prepreg employing unique annular plate geometries. The effect of processing parameters (temperature, velocity, and normal force) on the frictional response of a carbon fiber prepreg was studied. Moreover, utilizing custom designed plate geometries coupled with optically transparent fixtures allowed for in-situ quantification of the prepreg-rigid surface contact area along with simultaneous characterization of the process parameter-dependent frictional mechanisms. Our findings highlight the reduction in rictional forces with increasing temperature, attributed to the increased resin flowability, while increases in sliding rates resulted in a pronounced increase in the frictional forces. The effect of applied load on the frictional characteristics was more complicated due to contributions from both the adhesive and normal forces. Finally, the results were interpreted in light of the contact area measurements performed at different temperatures, normal force, and sliding rate.

1. Introduction

Carbon fiber reinforced plastics (CFRPs) have gained significant attention in the aviation industry due to their high stiffness-to-weight ratio, fatigue performance, corrosion resistance, thermal stability, and low thermal expansion [1]. Thermosets are the most common polymer matrix for CFRPs, which are often manufactured using labor-intensive, traditional hand-laminating techniques that are followed by vacuum bagging or autoclave curing. Some disadvantages of traditional methods are the high labor costs and the susceptibility of fabrication to human error that can lead to formation of defects that reduce the part's final properties [2,3]. In recent years, automated material placement (AMP) has been developed and employed by the aviation industry to reduce the lay-up process times, improve the overall manufacturing reliability, and achieve cost efficiencies for large components [4]. Industrial manufacture of functional parts of epoxy-based thermosets pre-impregnated with

carbon fibers (prepregs) with optimized mechanical properties generally involve automated lay-up followed by curing in an autoclave [4,5]. Automated fiber placement (AFP), automated tape lay-up (ATL), and filament winding are common AMP techniques that apply prepregs on a tool in a layer-by-layer manner at defined orientations to form a laminate [6]. The benefits of AMP processes include high production volume, quality assurance, and reduction in labor costs, albeit with high installation costs due to infrastructure requirements [7].

In a typical ATL process (schematically represented in Fig. 1), a spool lays up the prepreg material, which is subsequently held on the mold surface by applying a designated compaction force using a compaction tool [8]. The material property that controls the adhesion of the prepreg laminate feed to the compaction tool and to subsequent plies is the prepreg tack [9]. Tack is a rather complex metric involving the ability to conform and wet an underlying layer coupled with the ability to resist detachment, either by adhesion or by cohesion. A number of methods

E-mail addresses: Davide.Defocatiis@nottingham.ac.uk (D.S.A. De Focatiis), mbortner@vt.edu (M.J. Bortner).

 $^{^*\ \} Corresponding\ author.\ Department\ of\ Chemical\ Engineering,\ Virginia\ Tech,\ Blacksburg,\ VA,\ 24061,\ USA.$

^{**} Co-corresponding author.)

have been used to characterize tack [10–13], and it is well established that prepreg tack is dependent on the viscoelastic properties of the resin at the conditions imposed by the ATL processing parameters [8,14,15]. The adhesion between the prepreg laminates and the compaction tool is dependent on the effective contact area between the mating surfaces [16]. The compaction force or pressure exerted by the tool head is an important parameter that controls both the tack [17] and the contact area [9]. In order to overcome problems encountered due to insufficient tack during layup, the temperature and feed rate [8,18] have been varied but the optimization of the processing parameters in industries is still largely done on a trial and error basis resulting in a significant amount of time and material wastage [8,19].

Improper selection of forming parameters can lead to defect generation during the manufacturing process, resulting in parts with reduced mechanical properties. During the forming processes, the friction between the layup tool and prepreg surface leads to the generation of stresses. The built-up stresses, if large enough to overcome tack, can result in wrinkling and undesired distortion in the finished part. Moreover, the prediction of wrinkle formation in a composite is a non-trivial task and generally requires computationally intensive finite element analysis and a sound understanding of the underlying physics [20–22]. Therefore, a thorough understanding of the effect of the processing parameters on the prepreg material properties and frictional mechanisms during a given lay-up process is of significant interest.

Relative sliding of a ply over a tool surface during forming can occur either through a frictional mechanism or through a shearing mechanism of a sufficiently tacky resin. Within the scope of our current work, we refer to the cause of such tool-ply slippage as an "apparent frictional force", that can originate due to friction or shear. Generally, ply-ply friction is higher than tool-ply friction and hence slippage is more likely to occur at the tool-ply interface. Such "frictional" behavior has been found to be strongly dependent on the forming temperature, sliding velocity, and normal pressure [23,24]. The tool-ply frictional behavior encountered during forming of glass fiber reinforced polypropylene (PP) was modeled based on the Reynolds' equation for lubrication in thin films [23]. Although the predictive model can be used to minimize friction during forming as well as to study the effects of processing parameters on the frictional response, experimental validation of the model was fairly limited [23]. The frictional behavior of PP-glass fabric was found to be dependent on both the resin viscosity and the extent of contact between the tool and the material [24]. A reduction in frictional forces was observed when transitioning from low to intermediate temperatures due to a reduction in resin viscosity, but at higher temperatures, direct contact between the tool and fiber was established, resulting in increased frictional forces [24]. Similar results were observed for thermosetting systems (carbon fiber-reinforced prepregs) where the frictional forces increase with temperature due to enhanced fiber-tool contact [25,26]. However, both of these studies only

investigated the effects of temperature and cure on the frictional properties of the prepregs. Böckl et al. [27] developed an online monitoring system for prepreg slit tapes and found that increasing velocity reduced the frictional force between the tool and the sample. Although such experiments and process monitoring techniques are useful characterization tools, they do not provide insights into the associated frictional mechanisms.

Another factor that can affect the tool-ply friction is the fiber weave and/or orientation, with tighter weaves resulting in higher frictional forces compared to unidirectional (UD) fabric [28,29]. Other factors affecting the frictional force between tool and ply include prepreg temperature prior to and during forming [24,30], tool material and surface finish, and type of release agent [31]. Tool speed, sliding velocity, tool temperature, and normal pressure were found to be the most influential factors when manufacturing composite materials [28].

Frictional measurements of woven fabrics can also vary widely depending on processing parameters, measurement technique, and instruments used [32]. Current frictional characterization techniques require complex custom instrumentation and often produce inconsistent results. For example, traditional pull-out and pull-through [33] measurements performed on PP/glass fabric sheets did not match with the results obtained using a commercial rheometer due to the limitations associated with the normal force and velocity achievable in the rheometer [34]. Using a modified rheometer setup to achieve a wider range of normal stresses, Kavenhpour and McKinley [35] studied the effects of applied load and sample gap on the frictional properties of a fluid-solid pair and obtained characterized tribological properties over a wide range of sliding velocities. Sun et al. [36] characterized the inter-ply friction of two types of carbon fiber prepregs employing a pull-through method. The frictional forces were found to be directly proportional to the surface roughness of the samples [36]. However, most of the existing techniques are directed towards thermoplastics and research related to monitoring the frictional properties of fiber-reinforced thermoset composites are fairly limited in the literature, most likely due to the poor understanding of the implications of a wide window of processing conditions including temperature and degree of cure on the viscosity of an uncured (or a B-staged) resin during a typical forming process.

In this work, we propose a test method to characterize the apparent frictional properties of unidirectional (UD) carbon fiber prepregs using torsional rheometry and monitor the effects of processing conditions on the frictional response to reflect the tool-ply interactions encountered during a typical lay-up process. The frictional sliding tests are conducted in a rheometer using a custom-designed, annular parallel plate geometry (the modified top plate of the rheometer mimicking the compaction tool of a typical ATL setup). The annular geometry produces a measurement that is averaged over all directions, and hence cannot distinguish between frictional sliding parallel to or perpendicular to the fiber

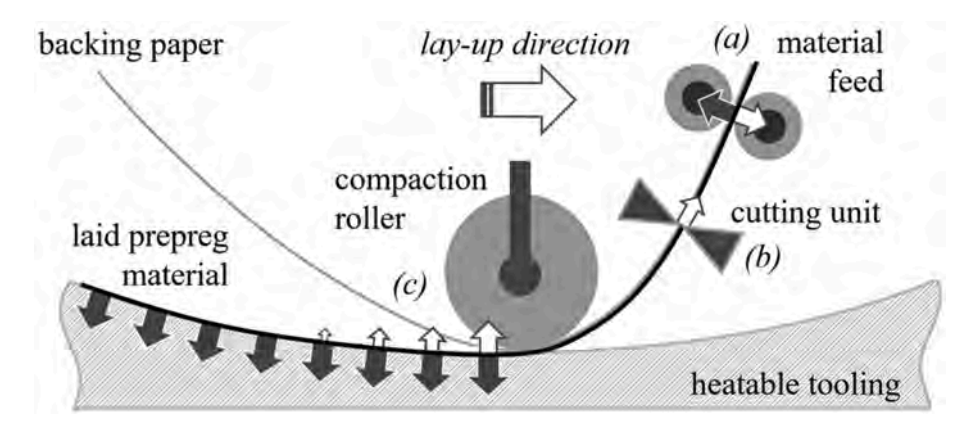


Fig. 1. A simplified schematic representation of the automated tape laying process (ATL) (Figure reproduced with permission from Ref. [9] and distributed under the terms of the Creative Commons CC BY license).

directions. Although this is a limitation of the technique, it circumvents a common problem with linear sliding experiments. Linear sliding experiments must, by virtue of their geometry, have a start and an end to the contact, and it is known that this can affect the measurements [36]. There has been contrasting reports in literature about the effect of fiber orientation affecting the frictional measurements of fabrics performed using linear techniques, some exhibit an effect of fiber orientation [31, 37] while others do not [30]. In the current manuscript, the effects of varying temperature, sliding velocity, and contact pressure on the frictional behavior of the prepreg fabric are evaluated.

Next, optically transparent annular acrylic plate fixtures were attached to the rheometer top plate to observe and quantify the contact area between the prepreg and rigid surface. Optical micrographs of the prepreg-acrylic interface were processed and analyzed to quantify the contact area for each sliding test. The frictional sliding results are interpreted in conjunction with the in-situ imaging results (quantification of the contact area) to provide key insights into interplay between surface contact and associated friction forces. In the ATL process, the friction between the tool and ply in different parts of the mold should be controlled and understood; too high a friction can result in increased interfacial stress transfer resulting in warpage and defects, whereas too low a friction force can result in the tool slipping over the surface of the ply and can lead to interlayer wrinkling in the finished composite parts [38,39]. The results from this study can aid to inform process parameter selection for a process such that frictional forces can be regulated to facilitate the manufacture of parts with minimal defects.

2. Materials and methods

2.1. Materials

Automotive grade UD carbon fiber prepregs (B-staged) were supplied by Hexcel, Duxford, UK. The prepreg was made from M77 epoxy resin at resin content of 38% by volume and 50K carbon fiber tow at an areal fiber density of 300 $\rm g/m^2$. Prepreg specimens with dimensions of 30 mm \times 30 mm were adhered to the rheometer bottom plate with an ethyl cyanoacrylate-based adhesive (Loctite® Super Glue Gel, Henkel) to ensure no slippage occurs between the bottom plate and prepreg surface. Fig. 2 represents the schematic of the experimental setup with the prepregs in between the rheometer plates.

2.2. Frictional sliding tests

A rheometer (Anton Parr MCR 302) fitted with a convection temperature chamber (CTD 450) was used with different annular plate geometries, as listed in Table S1 of the Supplementary section, to measure the frictional sliding properties of the UD prepreg material.

2.3. Effect of ring geometry

The sliding tests with the different geometries were performed maintaining controlled linear velocity (\overline{V}) and constant contact pressure (P), as dictated by Eqs. (1) and (2), respectively.

$$\overline{V} = \frac{\iint v dA}{\iint dA} = \frac{\int_0^{2\pi} \int_{R_1}^{R_2} \omega r^2 dr d\theta}{\int_0^{2\pi} \int_{R_1}^{R_2} r dr d\theta} = \frac{2\omega (R_2^3 - R_1^3)}{3(R_2^2 - R_1^2)}$$
(1)

$$P = \frac{F_N}{\pi (R_2^2 - R_1^2)} \tag{2}$$

where, ω is the angular sliding velocity, v is the linear velocity, F_N is the normal force (exerted by the rheometer plate on the surface of the prepreg samples) responsible for contact pressure generation, R_1 and R_2 are the inner and outer radii, respectively, of the annular plate geometries used. The required values of ω and F_N for the experiments are also listed in Table S1. The sliding tests for assessing the effect of annular plate geometry on the frictional behavior of prepregs were performed at a fixed temperature of 40 °C.

2.3.1. Effect of processing parameters

Prepreg samples were loaded onto the rheometer as highlighted in Fig. S1 of the supplementary information section. The samples were allowed to thaw to room temperature and then heated to the test temperature at a constant ramp rate of 5 °C/min to the desired temperature and then a constant normal force (F_N) was applied. A hold time of 30 s was applied (in order to minimize transient fluctuations to the temperature profile while limiting the effects of additional curing due to prolonged thermal exposure) before performing the frictional sliding tests at different angular velocities (ω) . After each run, the top and bottom plates were cleaned with acetone to remove any residual resin from the preceding experiment before mounting a fresh sample. The input variables for the sliding tests are tabulated in Table 1. The output results reported later in the manuscript are averages of three repeat measurements.

Table 1List of values of temperature, angular velocity, and normal force employed during the frictional sliding experiments.

Temperature (°C)	Angular velocity (mrad/s)	Normal force (N)
20, 30, 40, 50, 60, 70	1, 10, 100	5
20, 30, 40, 50, 60, 70	1, 3, 10, 30, 100	5
30, 40, 50	10	0.5, 2, 5

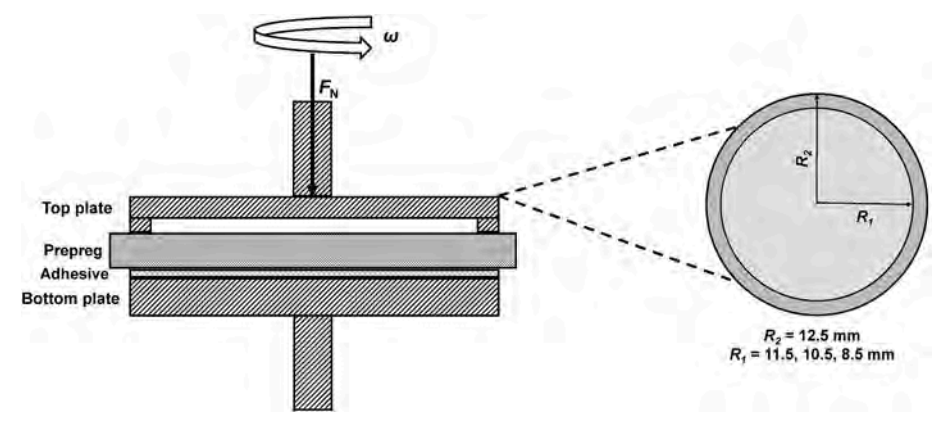


Fig. 2. Schematic representation of the rheometry experimental setup used for performing the frictional sliding experiments using an in-house annular plate geometry. The prepreg is attached to the bottom plate using a thin layer of adhesive and the annular top-plate exerts a constant normal force (F_N). During a typical frictional sliding experiment, the top-plate rotates over the prepreg surface at a constant angular velocity (ω). R_1 and R_2 are the inner and outer radii of the annulus, respectively. The dashed lines indicate a magnified view of the top-plates of the rheometer. In this study, annular plates having $R_2 \cdot R_1$ widths of 1 mm, 2 mm, and 4 mm were employed.

2.4. Prepreg-substrate interface imaging

2.4.1. Preparation of acrylic substrates for imaging

The experiments described in Section 2.2 were either performed on 25 mm aluminum plates (either solid or with different annular widths). However, such experiments are unable to provide information on how the processing parameters affects the contact area evolution between the rheometer plate and the prepreg surface. The objective of this section is to employ an acrylic element to generate comparable annular contact as obtained using the aluminum plates. The transparent acrylic fixture will provide a view of the interface between the prepreg and the rigid surface that can be subsequently imaged to evaluate the prepreg-rigid surface contact area. All the experiments related to the contact area characterizations were carried out using a modified top plate design as discussed below.

The frictional sliding tests for the contact area characterizations were performed using a detachable annular acrylic fixture (Figs. S2a and S2c of the Supplementary Information describes the design of this fixture) that was fixed to the rheometer plate. In order to accommodate the fixture within the rheometer, a top plate was also machined (the design of which is highlighted in Figs. S2b and S2d of the Supplementary Information). The acrylic fixture was prepared using a laser-cutter. Briefly (for the acrylic part), a square outline of 20 mm was laser cut (Trotec Speedy 100, Trotec Laser) on an acrylic sheet (POLYCASA® CAST), of 3 mm thickness, with two circular outlines of diameters of 18 mm and 14 mm respectively (40W, 2.5 mm/s, 5000 Hz). The protective film on the acrylic sheet was then removed from the parts except the portion that covered the annular region (~2 mm thickness). Next, the laser was used to engrave the exposed regions of the plate (1000W, 30 mm/s, 1000 PPI) and subsequently etch an outline (40W, 2.5 mm/s, 5000 Hz) on the annular region to ensure better surface finish. Finally, the laser was used to cut out the part from the acrylic sheet (100W, 0.90 mm/s, 5000 Hz) and the plate was washed in deionized water to remove any debris present on the surface. The plates were lightly polished using a dry and wet abrasive paper (MetPrep Ltd., Coventry, UK) (2500 grit and 4000 grit) to remove burrs. The finished part was then attached to the modified top plate and the protective film on the annular region was only removed just prior to the frictional sliding experiments.

The width of the laser-cut acrylic annulus was measured by capturing a high resolution image (2358 \times 3701 pixels) of the fixture using a scanner and subsequently analyzed using ImageJ software [40]. Ten measurements of the width of the annulus were taken at different locations on the circumference of the fixture, and it was found that the annular ring had an average width of 1.84 \pm 0.07 mm. The average outer and inner diameters of the plate were also measured and found to be 17.56 \pm 0.13 and 13.88 \pm 0.09 mm, respectively. These values were then used to calculate the normal force and angular velocity (using Eqs. (1) and (2)) required to maintain a constant contact pressure and constant linear sliding velocity mimicking the experimental conditions for the 25 mm aluminum plates with 1 mm wide annulus.

2.4.2. Optical microscopy and imaging procedure

The contact area between the prepreg and the rigid acrylic surface post-sliding was imaged using brightfield microscopy in reflection mode. After a typical frictional sliding test, the annular acrylic fixture was detached from the top plate, remaining in contact with the prepreg. The assembly consisting of the acrylic fixture, prepreg and lower rheometer plate was removed from the rheometer. The assembly was mounted on a locating template on a rotating microscope stage (Fig. S3 of the Supplementary Information section). An Olympus BX51 microscope equipped with an Infinity 2 digital camera was used to capture the contact area using a 4x objective lens. Individual micrographs were acquired along the circumference of the annular acrylic plate at 15° intervals resulting in a total of 25 micrographs for each specimen. An annular ring composite image was constructed by stitching the 25 micrographs using Microsoft Image Composite Editor software (Microsoft

ICE, version 2.0.3). Representative examples of an individual micrograph and a stitched composite image are illustrated in Fig. S4 of the Supplementary Information section.

2.4.3. Image processing procedure for determining contact area

Images were processed using MATLAB (Matlab 2019b) to determine the degree of intimate contact defined as the fraction of the annular area in contact between the prepreg and acrylic surface. The initial step consists of converting the composite image to a greyscale (8-bit) image. Regions of interest (ROI) were identified for each set of annular ring images to avoid arbitrary cropping of the images. The inner circumference of the annular ring image was approximated using a minimum of three user-defined points to identify the center coordinates of the ring. The outer circumference of the annular ring was calculated based on the measured width of the annulus. The annular ring ROI was determined by increasing and decreasing the inner and outer radii respectively by 0.3 mm to remove edge artifacts due to the acrylic cutting process (as illustrated in Fig. S5). The procedure to obtain the ROI provided a composite image with 722 pixels. Each test condition was represented by a single annular ring composite image.

The brightness histogram of the ROI is then computed and utilized to determine the threshold value to create a binary image (with only black and white pixels). When identifying the threshold value, the histograms for the greyscale images were modified to exclude the frequency count from the two extreme grey values: 0 and 255, corresponding to black and white pixels respectively [16]. Both of these grey values do not relate to features of interest in this work. Different histogram shapes were produced from the contact area pattern generated during the friction sliding test, and simple automatic methods were employed for threshold selection [16]. For unimodal histograms, the threshold value for binarization were obtained using the Triangle method, whereby a line is constructed between the minimum and peak value on the histogram and the furthest normal distance between this line and the histogram identifies the threshold value [41]. In the case of bimodal histograms, the Isodata method was used to determine the threshold value through iteratively identifying an average intensity value obtained from the two peak values until converging to the threshold value [42]. The contact area for each binarised image was determined by dividing the count of black pixels in the ROI by the total pixel count in the identical ROI.

3. Theory

3.1. Friction background: Contact area implications

The frictional force F_i between two surfaces sliding past each other under low normal forces is described by the classical equation developed by Bowden and Tabor [43]:

$$F_{\rm f} = \tau A_{\rm c} \tag{3}$$

where, τ is the critical shear stress and A_c is the true intimate contact area. It is well known that for adhesive and non-adhesive contacts the dependence of A_c on F_N is described by the Johnson-Kendall-Roberts (JKR) [44] and Hertz models [45], respectively, even during sliding. At increased F_N , there are additional contributions from forces originating due to friction as described by Amontons' law [46]. But for all practical applications, A_c between two solids is determined by the interaction of the surface roughness peaks, often referred to as single-asperity contacts [47,48]. Typically, A_c is orders of magnitude lower than the apparent area of contact [49,50] and is governed by the localized stresses at the contacts [51]. In the case of advanced manufacturing processes, A_c is the area that is wetted by the prepreg resin when the tool and sample are in contact [52–54]. The aforementioned theories agree on the importance of A_c in dictating how frictional mechanisms evolve between surfaces sliding past one another.

Experimental characterization to quantify A_c has proven to be quite challenging and limited studies have performed direct measurement of A_c [16,47,51,55–57].

3.2. Friction model development

In order to derive the relationships between the torque M measured by the rheometer during the sliding tests, the frictional force $F_{\rm f}$, and the coefficient of friction μ associated with the system under investigation, the following were assumed:

- Amontons' laws of friction are valid for the system. Therefore, the frictional force is directly proportional to the applied load and independent of the apparent area of contact between the concerned surfaces [46].
- When a constant normal force is applied, changes in frictional stress are due to changes in intimate contact area.
- The nominal frictional stress and resulting coefficient of friction are constant.

According to the classical Amontons-Coulomb's law that relates F_f with the applied F_N during the onset of relative motion between two solids,

$$F_f = \mu F_N \tag{4}$$

The normal force acting on a differential area dA of a surface due to a constant pressure P is given by

$$dF_N = PdA \tag{5}$$

The above equation is consistent with the classical friction theory described by Bowden and Tabor [49] which describes the nominal pressure generated as $P = F_N/A$. Under constant pressure as assumed for this analysis, an increase in F_N results in viscoelastic-plastic deformation and flow of the matrix and leads to an increase in F_N [51]. As highlighted in Fig. S6, the differential area can be expressed by the differential radial distance and differential circumferential length as follows

$$dA = rdrd\theta \tag{6}$$

Combining Eqs. (4)–(6), the expression for the differential frictional force (dF_f) associated with the differential area (dA) is given as

$$dF_f = \mu P r dr d\theta \tag{7}$$

For the frictional sliding tests, M required to rotate the rheometer top plate over a certain distance of the prepreg is recorded as a function of time. The differential torque dM for the required movement can be described by

$$dM = rdF_f = \mu Pr^2 dr d\theta \tag{8}$$

The total torque *M* required to move the top plate over a specified distance on the prepreg (or over a specified time-interval) can be obtained by integrating over the entire annular area as [58].

$$M = \mu P \int_{0}^{2\pi} \int_{R_1}^{R_2} r^2 dr d\theta = \frac{2\pi}{3} \mu P(R_2^3 - R_1^3)$$
 (9)

Eq. (5) can therefore be expressed as

$$P = \frac{F_N}{A} = \frac{F_f}{\pi \mu (R_2^2 - R_1^2)} \tag{10}$$

Substituting P from Eq. (10) into Eq. (9), the following equation is obtained for M as a function of F_f

$$M = \frac{2F_f(R_2^3 - R_1^3)}{3(R_2^2 - R_1^2)} \tag{11}$$

3.4. Re-arranging the above equation and solving for F_f

$$F_f = \frac{3M(R_2^2 - R_1^2)}{2(R_2^3 - R_1^3)} \tag{12}$$

Finally, substituting the value of F_f from Eq. (4) in the above equation leads to an expression that relates μ to M and F_N as

$$\mu = \frac{3M(R_2^2 - R_1^2)}{2F_N(R_2^3 - R_1^3)} \tag{13}$$

It is worth mentioning that to calculate μ , the maximum value of $F_{\rm f}$ is considered since it is inherently associated with the interactions due to the surface asperities that prevent relative motion between the two mating surfaces. A typical plot of torque and of frictional force versus time is illustrated in Fig. S7 of the Supplementary Information section.

4. Results and discussion

4.1. Frictional properties

4.1.1. Effect of ring geometry

Three different annular ring geometries and one solid plate were studied to understand the influence of the geometry on the frictional properties of the prepregs. The width of the annular ring ranged from 1 mm to 4 mm. A flat, solid 25 mm diameter parallel plate serving as a control was also employed in the study. Isothermal experiments were performed at 40 °C with constant mean sliding velocities and contact pressures (Table S1). Fig. 3a shows the maximum frictional force ($F_{f,max}$) increasing with the increase in the width of the annular ring. However, when scaled with the corresponding values of F_N , it is apparent that μ is independent of the geometry of the contact, as shown in Fig. 3b. The torque and frictional force measurements as a function of time for the different geometries are presented in Fig. S8 of the Supplementary Information section. It is worth mentioning that torque measurements for all the annular ring geometries (except the 1 mm width) and for the solid parallel plate approached the torque limit of the rheometer; however, they were still within the acceptable range. Therefore, for the frictional sliding experiments discussed in the following sections, the 25 mm parallel plate with 1 mm annular width was selected to allow probing a broader range of experimental conditions.

4.1.2. Effect of temperature

Temperature controls both the material properties and environmental conditions during a lay-up process. Typically, infrared heaters and/or heated tools are employed during lay-up of composites to improve adhesion to the tool or laminate [59]. The effect of temperature on the frictional properties of the prepregs as a function of different sliding velocities is highlighted in Fig. 4. The normal force was maintained at 5 N for all the test conditions corresponding to an average pressure of 66.4 kPa. In order to limit cure initiation in the prepreg, the maximum temperature investigated was 70 °C, as recommended from the manufacturer's data sheets. For the relatively low temperature (20 and 30 °C) samples, the values of μ are significantly higher than at higher temperatures. A possible explanation is that the adhesive contributions of the prepreg resins dominate due to insufficient wetting of the prepregs. Therefore, a large frictional force is required to "break" the bonds formed between the rheometer top plate and the prepreg sample prior to relative movement between the surfaces in contact [36]. On the other hand, an increase in processing temperature generally leads to lower apparent frictional values due to a decrease in viscosity; however, the drop in viscosity also leads to an increase in resin flowability, and hence a significant increase in surface wetting, resulting in higher frictional forces [34,60]. Prepreg tack is an important material parameter that controls the frictional behavior by dictating the adhesion between the tool and the sample [9]. Reduction in tack has been reported with

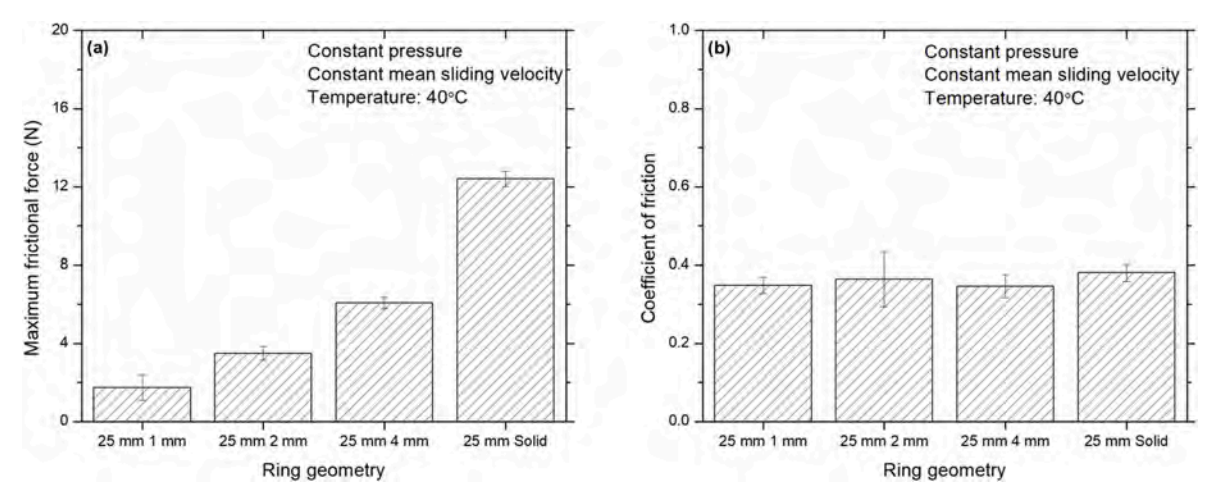


Fig. 3. (a) Maximum frictional force ($F_{f,max}$) as a function of different annular ring geometries (b) Effect of the different annular ring geometries on the coefficient of friction (μ). All the tests were performed at 40 °C while maintaining constant contact pressure (66.4 kPa). The angular velocities for the 1 mm, 2 mm, and 4 mm annular plates were 10 mrad/s, 10.4 mrad/s, and 11.3 mrad/s, respectively while that for the solid plate was 14.4 mrad/s.

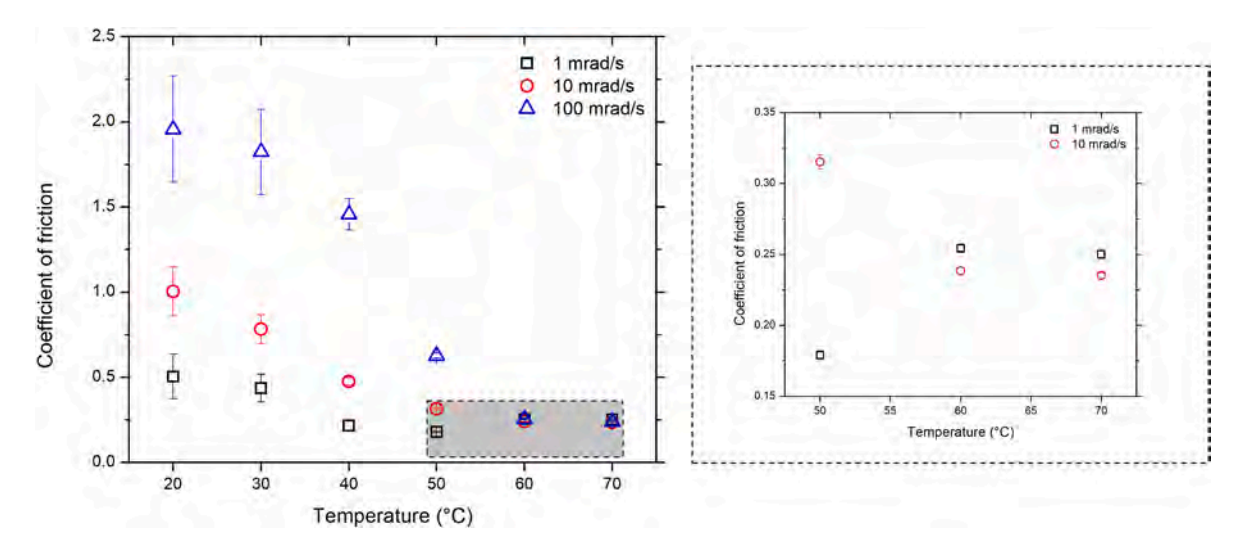


Fig. 4. Effect of temperature on the coefficient of friction between the rheometer plate and prepreg samples under 5 N normal force as a function of different angular velocities. The figure to the right represents the same plot but zoomed in the shaded region of the figure to the left between 50 °C and 70 °C for angular velocities of 1 mrad/s and 10 mrad/s. The results were obtained using a 25 mm parallel plate with a 1 mm wide annular ring geometry.

increasing temperature [15,61], that is likely to cause a reduction in the frictional force, a trend consistent with our findings. Similar reduction in frictional forces were reported on thermoset prepregs from Hexcel by Martin et al. [62] who found that both resin viscosity and its distribution on the prepreg surface influenced the frictional response.

An alternative interpretation for the results can be postulated from the Stribeck friction theory [63] that relates resin viscosity, sliding velocity, and normal force with the coefficient of friction. The theory has three main regimes: boundary, mixed, and elasto-hydrodynamic lubrication, all controlled by the relative velocity and degree of contact, here between the surfaces of the rheometer plate and prepreg. The high values of frictional force and coefficient of friction at lower temperatures (20–30 °C) may be indicative of the hydrodynamic lubrication regime (i. e., higher viscosities) whereas the subsequent decrease in the frictional force may be characteristic of a mixed lubrication regime where the resin (due to thermally activated mobility) is transported between the surface asperities facilitating relative motion.

An interesting deviation is observed for the samples tested at the lowest sliding velocity (1 mrad/s) where μ increases with temperature after 50 °C, as shown in Fig. 4. Previous research groups have postulated the reason behind this deviation to be the direct contact between the tool

and fiber due to the resin flow [24,34]. Another important finding is that after 50 °C the values of μ decrease when the angular velocity is increased from 1 mrad/s to 10 mrad/s; likely due to a limited time window for achieving sufficient contact and wetting. This trend is consistent with the work by Böckl et al. [27] where an increase in sliding rate resulted in decrease of the transverse frictional force for prepreg slit tapes during lay-up using AFP.

4.1.3. Effect of sliding velocity

Fig. 5 illustrates the transition of the frictional response from mixed lubrication to the elasto-hydrodynamic lubrication regime as a function of the sliding velocity at different temperatures. The effect of sliding velocity on the frictional sliding properties of prepregs was studied at different temperatures under a constant normal force of 5 N (nominal pressure of 66.35 kPa). The corresponding plots for maximum frictional force as a function of sliding velocity are presented in Fig. S9 of the Supplementary information section. An overall increase in μ is observed with the increase in sliding velocity in the temperature range 20–50 °C, which is representative of a system undergoing a transition from the mixed lubrication regime to the elasto-hydrodynamic regime in a Stribeck curve [34,36]. Values of μ are found to decrease with temperature

A. Das et al. Composites Part B 236 (2022) 109777

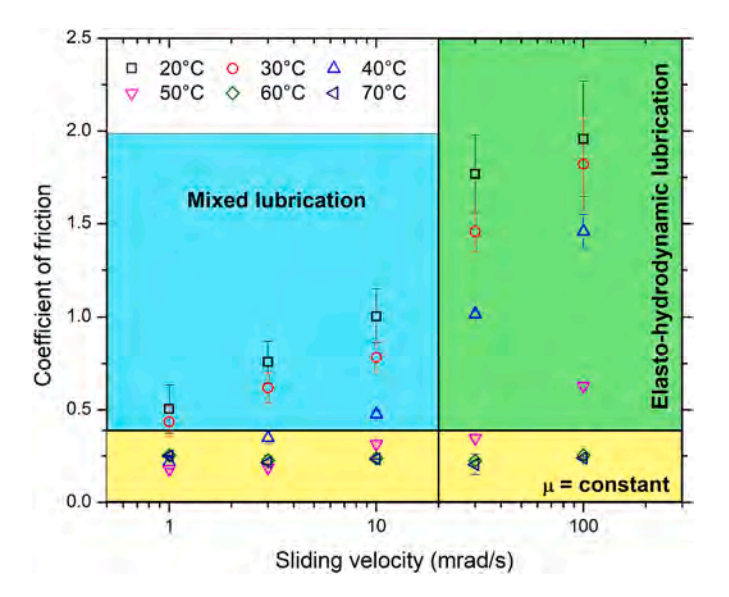


Fig. 5. Effect of sliding velocity on the coefficient of friction between the rheometer plate and prepreg samples under 5 N normal force as a function of temperature. The transition between the different regimes of the Stribeck curve is highlighted as well. The values of μ at higher temperatures (60–70 °C) are invariant of the sliding velocity.

in the elasto-hydrodynamic regime at comparable angular velocities likely due to the reduction in resin viscosity at increased temperatures. At slightly higher temperatures 60 $^{\circ}\text{C}$ and 70 $^{\circ}\text{C}$ the apparent frictional properties appear to become less dependent of the sliding velocity.

Another reason behind the results could be the faster interaction between the rheometer top plate and the prepreg sample at higher sliding velocities, which can lead to interlocking of the fibers which would, in turn, require more force to overcome friction to initiate relative motion. Similar results (increased sliding rates resulting in higher frictional forces) were reported by Ramkumar et al. [64] while investigating the frictional behavior of nonwoven fabrics using a sliding friction apparatus. Kim et al. reported a similar increase in frictional resistance and μ with the increase in sliding velocity for UD carbon/epoxy prepregs [65]. In order to further rationalize the results obtained in this work, the dependence of μ on the sliding velocity is modeled using the rate and state friction laws [66,67] as

$$\mu = A + Blog v + Clog t \tag{14}$$

where A, B, and C are all material constants specific to the system under investigation, ν is the sliding velocity, and t is a characteristic dynamic timescale. Under steady state assumption, Eq. (14) simplifies to the following

$$\mu_{ss} = A + B \log v \tag{15}$$

If B > 0, the coefficient of friction increases with velocity, a phenomenon referred to as velocity strengthening [67]. From the data presented in Fig. 5 it is apparent that there is a transition in the frictional behavior as the sliding velocity increases from intermediate to high values for the temperature range of 20-40 °C. Table 2 presents the values of the material dependent constants A and B for two different regimes: low to intermediate (1-10 mrad/s) and intermediate to high (10-100 mrad/s) sliding rates for test temperatures 20-40 °C (the corresponding linear fits are presented in Fig. S10 of the Supplementary Information section). As evident from the non-negative values of B, the prepreg is in a velocity strengthening regime over the velocities investigated in this study within the temperature window of 20-50 °C. The origin of the transition (disappearance of the two-slope nature of μ as a function of log v) occurring between 40 °C and 60 °C is likely linked to the variations in surface and volume activation energies (both strongly dependent on the thermal energy input to the system) [68,69]. In addition, the increase in μ at high sliding velocities can be attributed to the localized inertia effects occurring within the contact asperities. Therefore, the frictional mechanism of CFRPs during the manufacturing can be controlled by tuning the sliding velocity.

Finally, from the perspective of prepreg tack, previous works have shown tack to increase as the interface between the prepreg and the tool is subjected to faster rates [70,71] in processes similar to ATL. Increased

Table 2Values of material constants A & B obtained by linear fitting of Eq. (15) to the data obtained from the frictional sliding experiments performed at different angular velocities in the temperature range of 20–40 °C.

Temperature (°C)	20	30	40	20	30	40
Angular velocity (mrad/s)	1–10			10–100		
A	$\begin{array}{c} 0.51 \\ \pm \ 0.01 \end{array}$	$\begin{array}{c} 0.44 \\ \pm \ 0.01 \end{array}$	$\begin{array}{c} 0.23 \\ \pm \ 0.01 \end{array}$	$\begin{array}{l} -0.06 \\ \pm \ 0.48 \end{array}$	$\begin{array}{l} -0.40 \\ \pm \ 0.29 \end{array}$	$\begin{array}{c} -0.61 \\ \pm \ 0.10 \end{array}$
В	$\begin{array}{c} 0.50 \\ \pm \ 0.02 \end{array}$	$\begin{array}{c} 0.35 \\ \pm \ 0.02 \end{array}$	$\begin{array}{c} 0.26 \\ \pm \ 0.01 \end{array}$	$\begin{array}{c} 1.11 \; \pm \\ 0.37 \end{array}$	$\begin{array}{c} 1.20\ \pm \\ 0.23\end{array}$	$\begin{array}{c} 1.10\ \pm\\ 0.08\end{array}$
R^2	0.997	0.993	0.998	0.803	0.931	0.99

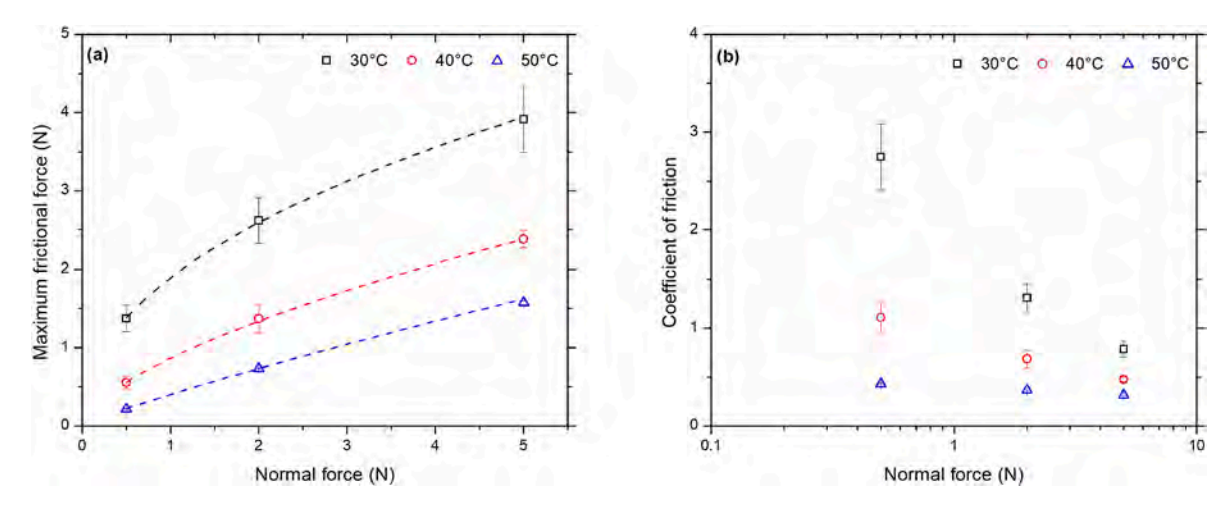


Fig. 6. (a) Variation in the maximum frictional forces as a function of applied normal force at different temperatures obtained from frictional sliding experiments performed at 10 mrad/s. The dashed lines represent the non-linear fits to the data using Eq. (16); (b) Corresponding effect of temperature on the coefficient of friction values as a function of normal force.

tack can likely indicate more adhesion between the contact surfaces, requiring more force to initiate relative motion. Therefore, the increasing trend in μ with sliding velocity is further justified.

4.1.4. Effect of normal force

In a typical lay-up process, the adhesion between the tool and prepreg is of paramount importance in order to ensure process optimization. Contact pressure or applied load during the lay-up process directly controls the extent of the aforementioned area of contact. The effect of normal force (and hence average contact pressure) was investigated at a constant sliding rate of 10 mrad/s in the temperature range of 30–50 $^{\circ}$ C. Fig. 6 highlights the variation in maximum frictional force and the corresponding μ between the rheometer top plate and the prepreg sample. With the increase in applied load, an overall increase in the maximum frictional force is observed. In this region, the surface roughness of the prepregs are negligible compared to the resin thickness and hence the values of μ are dictated by the shearing of the resin [72]. The values of μ decrease with increasing normal force and approach a minimum plateau value. At low normal forces, fibers can interlock with each other forming a rough contact surface. But with the increase in normal force, both the fibers and any existing interfacial asperities are compacted resulting in a smoother surface and hence lower values of coefficients. The behavior is indicative of elasto-hydrodynamic lubrication regime of the Stribeck curve where an increase in normal force (and hence contact pressure) results in lower values of μ . The findings are in agreement with reported work on UD carbon/epoxy prepregs [73] and polyester fabrics [74]. Previous research on UD fiber reinforced thermoplastic composites report similar decreases in μ as the applied load increases [30,31]. Tribological measurements performed on CFRP composites [75] and metals [76] further substantiate our findings (decreasing trend of μ against F_N). The values of μ decreases as the test temperature increases from 30 to 50 °C for the reasons discussed in Section 4.1.2.

The relationship between the frictional force and normal load is expressed using the following power-law equation [64]:

$$F_f = CF_N^n \tag{16}$$

where, C (Pa¹⁻ⁿ) and n are the friction parameter and friction index respectively, while a normalized friction factor (R) has been defined to be a ratio between C and n [64]. Table S2 in the supplementary information section lists the values of C and n obtained by fitting the values of frictional force as a function of normal force data. The experimental data is in agreement consistent with the power law model. The non-linear increase in frictional force indicates that the frictional behavior cannot

be described solely using Amontons' law [77] that assumes constant surface contact at varying contact pressures. As will be discussed in the following sections, the contact area between the surfaces does not remain constant and is highly dependent on the processing parameters. A better depiction of the normal force dependence of the frictional behavior can be achieved by considering both adhesive forces and applied load [77].

The coefficient of friction vs. normal force are also fitted to a power law relation ($\mu \sim F_N^m$) to check the extent of the dependence. At lower temperatures (30 °C) it is seen that μ scales with $F_N^{-0.54}$; however, with increase in temperature this dependence weakens to the extent that at 50 °C μ scales as $F_N^{-0.13}$. The lower values of the power law exponent with increasing temperature are indicative of the lower force requirements for the material to conform due to a reduction in viscosity. The fits to the power law model ($\mu = \mu_0 F_N^m$) are illustrated in Fig. S11 of the supplementary information section with the relevant model parameters listed in Table S3.

4.2. Contact area evolution

The sliding experiments were repeated to evaluate the contact area using the transparent acrylic fixtures attached to the rheometer top-plate to allow for imaging after each sliding test. The obtained images were then processed to quantify the area of contact between the acrylic fixture and the prepreg surface. In order to keep the contact pressure and mean sliding velocity as close as possible to those experienced by the prepreg sample during a typical frictional sliding test ($\omega=10$ mrad/s & $F_{\rm N}=5$ N), the normal force and angular sliding velocity for the acrylic annular fixtures were calculated using Eqs. (1) and (2). as 6 N and 15.2 mrad/s respectively.

The frictional measurements performed using the 25 mm parallel plate with 1 mm annular width was compared with that obtained using the acrylic plate fixture. The torque and frictional force profiles of the two geometries as a function of sliding time are presented in Fig. S12 of the Supplementary information section. Using Eq. (13), the values of the coefficient of friction ($\frac{F_{f,max}}{F_N}$) at 20 °C (under constant contact pressure and mean linear velocity) from using these two geometries are 1.04 \pm 0.14 and 1.07 \pm 0.04, respectively. Since the results between the geometries are comparable, a series of experiments were performed using the acrylic fixtures in an effort to decouple the individual effects of the process parameters on the contact area evolution during and after the frictional sliding experiments. Immediately after testing, the surface was imaged through the annulus of the acrylic fixture and the obtained images were stitched to obtain a composite image for further image

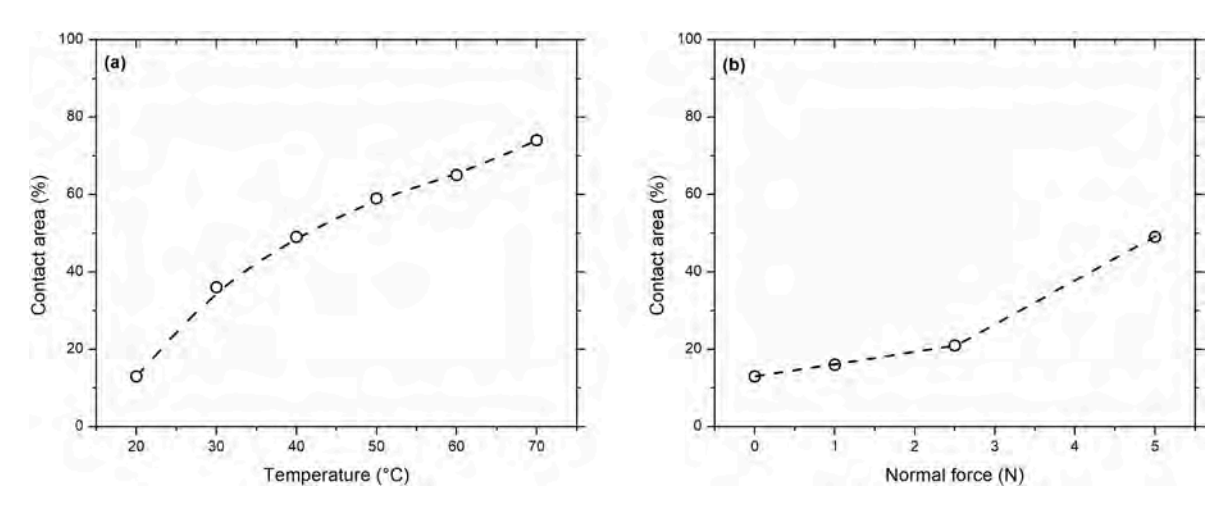


Fig. 7. (a) Effect of temperature on the contact area between the acrylic fixture and the prepreg samples (15.2 mrad/s and 6 N normal force). The dashed lines serve as a guide for highlighting the increasing trend; (b) Effect of normal force on the contact area between the acrylic fixture and the prepreg samples at 40 °C. The dashed lines indicate the sub-linear increase in contact area with normal force.

processing for contact area evaluation following the procedure outlined in Section 2.3.3 (Fig. S13 of the Supplementary Information section).

4.2.1. Effect of temperature and normal force

A series of sliding experiments were performed using the transparent acrylic fixture at different temperatures and different normal force while applying a constant angular velocity 15.2 mrad/s. Fig. 7a highlights the change in contact area as a function of temperature; it is apparent that the contact area increases with the increase in test temperature. The reduction in resin viscosity at elevated temperatures increases molecular mobility that leads to an increase in contact area between the surfaces.

The dependence of contact area on normal force has also been characterized at 40 °C under a sliding velocity of 15.2 mrad/s. As highlighted in Fig. 7b, the contact area increases slowly in the region of low normal forces (0–2.5 N) and then a more significant increase is observed as the normal force increases to 5 N. The compaction pressure increases with loading, resulting in an increase in the true contact area between the prepreg layer and acrylic surface. Hence, increasing compaction pressure effectively increases the maximum frictional force (as shown in Fig. 6a). Moreover, the sub-linear increase in contact area with the applied load, contrary to Amontons' law, is evidence of strain hardening as reported in a recent study by Weber et al. [55]. Deviations from the classical behavior may be due to the surface roughness present on the prepreg samples that allows only a fraction of the nominal area to come into contact, leading to high contact pressures.

4.2.2. Effect of sliding

In the absence of both sliding and applied normal force, although the weight of the upper 25 mm removable rheometer plate (4.21g) along with the acrylic fixture (2.14g) was still applied on the prepreg, the evolution of contact area is only temperature dependent, and exhibits an increasing trend as temperature increases due to more interfacial area being wetted by the resin given the lower viscosity. For the "no-load" case, the tests were performed without applying any external normal force (through the rheometer) and the acrylic fixture was kept on top of the prepreg surface for 10s (same duration as the tests described in the previous sections) at different temperatures. Fig. 8a displays the influence of normal force and temperature in the absence of sliding on the contact area measurements. The application of normal force does not affect the contact area at ambient temperatures but at higher temperatures, the effect of F_N is more pronounced and results in an increase in contact area by ~34-65% with respect to the experiments performed with no normal force. This is likely attributed to higher normal forces that squeezes out the resin (sandwiched between the rheometer plate

and carbon fiber tows). Since the plate and tow are in direct contact with each other, the effect of normal force on both the contact area and the frictional force is more pronounced.

Next, we performed interrupted sliding experiments at a specified sliding condition (40 °C, 15.2 mrad/s; & 6 N) but instead of running the test for the entire time period, the tests were interrupted at periodic time intervals to gauge the effect of sliding time on the evolution of contact area between the prepreg and the modified to-plate fixture. Fig. 8b represents the change in contact area as a function of sliding time. The contact area increases rapidly and reaches a plateau, suggesting that most of the changes take place at shorter timescales. The applied load is enough to elastically deform the asperities between the prepreg and the rheometer plate to varying extents. Due to the non-uniform nature of the surface roughness in most materials, the localized stresses (induced due to $F_{\rm N}$) can be very close to the yield stress of the materials under investigation [55,78,79]. Creep deformation is common in materials in contact under such elevated local stresses and leads to the increase in $A_{\rm C}$ with time (t) [50,80,81], governed by a classical logistic equation given by

$$A_c = \frac{a}{1 + e^{-k(t - t_c)}} \tag{17}$$

where, a, k, and t_c are model constants. The contact area evolution data with respect to time is in good agreement ($R^2=0.996$) with a traditional logistic model as shown in Equation (17). The value of the mode parameters a, k, and t_c are calculated to be $49.3\pm0.7~\mathrm{m}^2$, $1.02\pm0.07~\mathrm{s}^{-1}$, and $0.96\pm0.06~\mathrm{s}$, respectively.

5. Conclusions

A simple method to characterize tool-ply friction in fiber-reinforced composites using a rheometer setup with annular-plate geometry has been developed. The effects of processing variables on the frictional properties of carbon fiber prepregs have been studied. Increasing temperature reduces the viscosity of the prepreg resin, leading to a reduction in frictional forces. It is likely that the reduction in prepreg tack at higher temperatures lowers adhesive contributions and results in lower values of coefficients of friction. However, an increase in sliding velocity increases frictional forces, consistent with the transition from the mixed lubrication to the elasto-hydrodynamic lubrication regime of a Stribeck curve. Furthermore, the non-linear increase in frictional force with normal force suggests that the material is exhibiting strain hardening behavior and indicates that Amontons' law is unable to describe the frictional dynamics of prepreg composites. The coefficient of friction

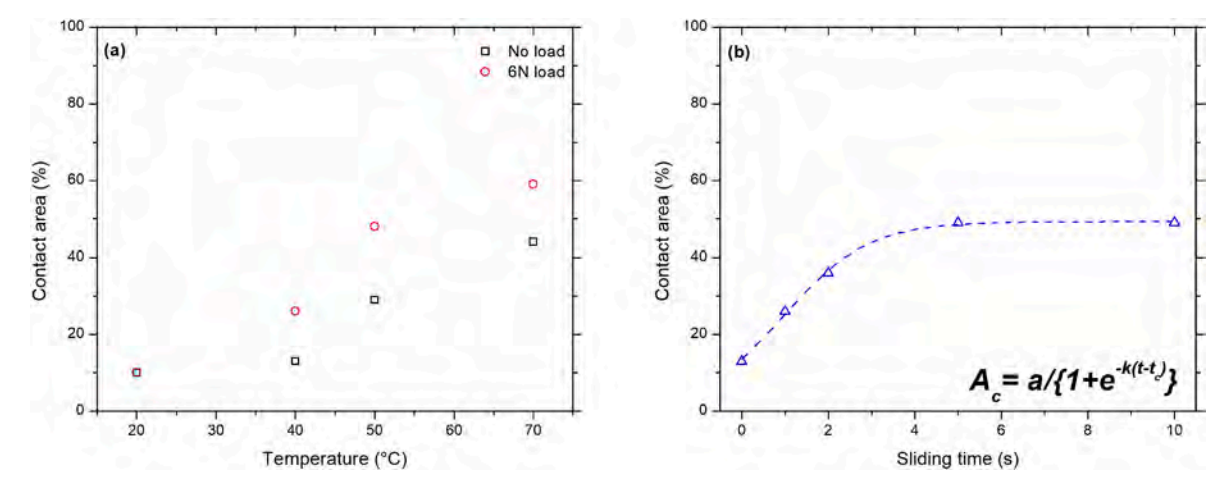


Fig. 8. (a) Contact area measurements without sliding in the presence and the absence of applied load carried out at different temperatures; (b) Effect of time of sliding on the contact area evolution during a typical frictional sliding experiment; the dashed lines indicate the non-linear fit to the data obtained using Eq. (17). Experiments were performed at 40 °C, 15.2 mrad/s sliding velocity, and 6 N normal force.

decreases with increasing normal force, suggesting hydrodynamic lubrication characteristics. From the point of view of ATL, a combination of higher temperatures (40-60 °C) under constant normal load and sliding velocity can help reduce warpage in the manufactured parts while slippage between the tool and prepreg material can be limited at higher sliding velocities at constant temperature and normal force. Although we probed a limited processing window within the scope of the current research, a broader understanding of the optimum processing conditions can be obtained by exploring both temperature and velocity ranges since it has been previously reported that time-temperature superposition applies to these processes [82,83]. Such an analysis will assist in establishing the link between prepreg tack and friction in order to limit defect formation in the manufactured parts. Moreover, it is possible weaves will exhibit similar frictional response and trends as highlighted in this work, provided the tack findings for the concerned weave are comparable to a unidirectional prepreg.

In order to better comprehend the frictional response of the prepregs, contact area between the surfaces was quantified using a custom acrylic attachment to the top plate of the rheometer that facilitated the imaging of the prepreg surface after each test. Temperature, applied load, and sliding time all affects the contact area to varying extents and the observed behavior is attributed to the combined effect of all these processing conditions. High contact pressures can induce creep deformation in the samples leading to an increase in contact area with time.

The approach outlined in the paper is applicable to a range of composite processing methodologies involving unidirectional plies and can be leveraged for ATL processing. It is worth mentioning that the frictional responses as a function of processing conditions discussed in this study can be utilized to control friction depending on the end goal of a selected processing technique. The results obtained from this study can lead to the development of physics-based process parameter optimization for the composite layup process thereby ensuring large scale defect free manufacturing of carbon fiber reinforced composites. The major beneficiaries from such research will be the industries employing material placement where process automation is still in its infancy, and where a sound understanding of the underlying physics to optimize processes is greatly desired.

Credit authorship contribution statement

Arit Das: Conceptualization, Data curation, Formal analysis, Investigation, Methodology, Software, Validation, Visualization, Writing original draft; **Gabriel Y.H. Choong:** Methodology, Software, Visualization, Writing – review & editing; **David A. Dillard:** Conceptualization, Supervision, Writing – review & editing; **Davide S.A. De Focatiis:** Conceptualization, Funding acquisition, Project administration, Resources, Supervision, Writing – review & editing; **Michael J. Bortner:** Conceptualization, Funding acquisition, Project administration, Resources, Supervision, Writing – review & editing.

Declaration of competing interest

The authors declare that they have no known competing financial interests or personal relationships that could have appeared to influence the work reported in this paper.

Acknowledgements

The lead author would like to acknowledge funding from the Adhesive Manufacturers Association Adhesive and Sealant Science scholarship from the Macromolecules Innovation Institute (MII) at Virginia Tech. The funding for the research conducted at University of Nottingham was provided though the International Research Experience for Students (IRES) program at Virginia Tech. The IRES program is funded though NSF Award 1261162. The authors would also like to thank Ivan Q. Vu and Kathleen J. Chan for their contributions that laid the

groundworks for this research. Finally, the collaborative infrastructure at Virginia Tech focused across the spectrum of polymer science and engineering provided by the MII at Virginia Tech is gratefully acknowledged.

Appendix A. Supplementary data

Supplementary data to this article can be found online at https://doi.org/10.1016/j.compositesb.2022.109777.

References

- [1] Das TK, Ghosh P, Das NC. Preparation, development, outcomes, and application versatility of carbon fiber-based polymer composites: a review. Adv Compos Hybrid Mater 2019;2:214–33. https://doi.org/10.1007/s42114-018-0072-z.
- [2] Campbell Jr FC. Manufacturing technology for aerospace structural materials. Elsevier; 2011.
- [3] Lindbäck JE, Björnsson A, Johansen K. New Automated Composite Manufacturing Process: : is it possible to find a cost effective manufacturing method with the use of robotic equipment?. 2012. p. 523–31.
- [4] Frketic J, Dickens T, Ramakrishnan S. Automated manufacturing and processing of fiber-reinforced polymer (FRP) composites: an additive review of contemporary and modern techniques for advanced materials manufacturing. Add. Manufactur. 2017;14:69–86. https://doi.org/10.1016/j.addma.2017.01.003.
- [5] Bajpai PK, Singh I. Reinforced polymer composites: processing, characterization and post life cycle assessment. John Wiley & Sons; 2019.
- [6] Jawaid M, Thariq M. Sustainable composites for aerospace applications. Woodhead Publishing: 2018.
- [7] Grimshaw MN, Grant CG, Diaz JML. Advanced technology tape laying for affordable manufacturing of large composite structures. International SAMPE Symposium and Exhibition; 2001. p. 2484–94. Long Beach, CA: Citeseer.
- [8] Crossley RJ, Schubel PJ, De Focatiis DSA. Time-temperature equivalence in the tack and dynamic stiffness of polymer prepreg and its application to automated composites manufacturing. Compos Appl Sci Manuf 2013;52:126–33. https://doi. org/10.1016/j.compositesa.2013.05.002.
- [9] Budelmann D, Schmidt C, Meiners D. Prepreg tack: a review of mechanisms, measurement, and manufacturing implication. Polym Compos 2020:1–19. https://doi.org/10.1002/pc.25642.
- [10] Tse MF. Studies of triblock copolymer-tackifying resin interactions by viscoelasticity and adhesive performance. J Adhes Sci Technol 1989;3:551–70. https://doi.org/10.1163/156856189X00407.
- [11] Gdalin BE, Bermesheva EV, Shandryuk GA, Feldstein MM. Effect of temperature on probe tack adhesion: extension of the Dahlquist criterion of tack. J Adhes 2011;87: 111–38. https://doi.org/10.1080/00218464.2011.545325.
- [12] Crossley RJ, Schubel PJ, Warrior NA. The experimental determination of prepreg tack and dynamic stiffness. Compos Appl Sci Manuf 2012;43:423–34. https://doi. org/10.1016/j.compositesa.2011.10.014.
- [13] Tonye DM, Gautier KB. Influence of the reinforcement on prepreg tack. Polym Compos 2021;42:4795–803. https://doi.org/10.1002/pc.26188.
- [14] Crossley RJ, Schubel PJ, Warrior NA. The experimental characterisation of prepreg tack. In: The 17th International Conference on composite materials (ICCM-17); 2009
- [15] Putnam JW, Seferis JC, Pelton T, Wilhelm M. Perceptions of prepreg tack for manufacturability in relation to experimental measures. Sci Eng Compos Mater 1995;4:143–54.
- [16] Choong GYH, Endruweit A, De Focatiis DSA. Analysis of contact area in a continuous application-and-peel test method for prepreg tack. Int J Adhesion Adhes 2021;107:102849. https://doi.org/10.1016/j.ijadhadh.2021.102849.
- [17] Endruweit A, Choong GYH, Ghose S, Johnson BA, Younkin DR, Warrior NA, et al. Characterisation of tack for uni-directional prepreg tape employing a continuous application-and-peel test method. Compos Appl Sci Manuf 2018;114:295–306. https://doi.org/10.1016/j.compositesa.2018.08.027.
- [18] Gutowski TG, Bonhomme L. The mechanics of prepreg conformance. J Compos Mater 1988;22:204–23. https://doi.org/10.1177/002199838802200301.
- [19] Lichtinger R, Hörmann P, Stelzl D, Hinterhölzl R. The effects of heat input on adjacent paths during Automated Fibre Placement. Compos Appl Sci Manuf 2015; 68:387–97. https://doi.org/10.1016/j.compositesa.2014.10.004.
- [20] Xie N, Smith RA, Mukhopadhyay S, Hallett SR. A numerical study on the influence of composite wrinkle defect geometry on compressive strength. Mater Des 2018; 140:7–20. https://doi.org/10.1016/j.matdes.2017.11.034.
- [21] Boisse P, Hamila N, Vidal-Sallé E, Dumont F. Simulation of wrinkling during textile composite reinforcement forming. Influence of tensile, in-plane shear and bending stiffnesses. Compos Sci Technol 2011;71:683–92. https://doi.org/10.1016/j. compscitech.2011.01.011
- [22] Guzman-Maldonado E, Wang P, Hamila N, Boisse P. Experimental and numerical analysis of wrinkling during forming of multi-layered textile composites. Compos Struct 2019;208:213–23. https://doi.org/10.1016/j.compstruct.2018.10.018.
- [23] ten Thije RHW, Akkerman R, Ubbink M, van der Meer L. A lubrication approach to friction in thermoplastic composites forming processes. Compos Appl Sci Manuf 2011;42:950–60. https://doi.org/10.1016/j.compositesa.2011.03.023.
- [24] Lebrun G, Bureau MN, Denault J. Thermoforming-stamping of continuous glass fiber/polypropylene composites: interlaminar and tool-laminate shear properties.

- J Thermoplast Compos Mater 2004;17:137–65. https://doi.org/10.1177/
- [25] Twigg G, Poursartip A, Fernlund G. An experimental method for quantifying tool–part shear interaction during composites processing. Compos Sci Technol 2003;63:1985. https://doi.org/10.1016/S0266-3538(03)00172-6. 2002.
- [26] Ersoy N, Potter K, Wisnom MR, Clegg MJ. An experimental method to study the frictional processes during composites manufacturing. Compos Appl Sci Manuf 2005;36:1536–44.
- [27] Böckl B, Jetten C, Heller K, Ebel C, Drechsler K. Online monitoring system for the tack of prepreg slit tapes used in automated fiber placement. In: ECCM18-18th European Conference on composite materials; 2018.
- [28] Gorczyca JL, Sherwood JA, Liu L, Chen J. Modeling of friction and shear in thermostamping of composites-part I. J Compos Mater 2004;38:1911–29.
- [29] Fetfatsidis KA, Jauffrès D, Sherwood JA, Chen J. Characterization of the tool/fabric and fabric/fabric friction for woven-fabric composites during the thermostamping process. Int J Material Form 2013;6:209–21. https://doi.org/10.1007/s12289-011-1072.5
- [30] Gorczyca-Cole JL, Sherwood JA, Chen J. A friction model for thermostamping commingled glass-polypropylene woven fabrics. Compos Appl Sci Manuf 2007;38: 393–406. https://doi.org/10.1016/j.compositesa.2006.03.006.
- [31] Murtagh AM, Lennon JJ, Mallon PJ. Surface friction effects related to pressforming of continuous fibre thermoplastic composites. Compos Manuf 1995;6:169–75. https://doi.org/10.1016/0956-7143(95)95008-M.
- [32] Sachs U, Akkerman R, Fetfatsidis K, Vidal-Sallé E, Schumacher J, Ziegmann G, et al. Characterization of the dynamic friction of woven fabrics: experimental methods and benchmark results. Compos Appl Sci Manuf 2014;67:289–98.
- [33] ASTM 1894-14. Standard test method for static and kinetic coefficients of friction of plastic film and sheeting. West Conshohocken, PA: ASTM International; 2014. https://doi.org/10.1520/D1894-14.
- [34] Harrison P, Thije RT, Akkerman R, Long AC. Characterising and modelling tool-ply friction of viscous textile composites. World J Eng 2010;7:5–22.
- [35] Kavehpour HP, McKinley GH. Tribo-rheometry: from gap-dependent rheology to tribology. Tribol Lett 2004;17:327–35.
- [36] Sun J, Li M, Gu Y, Zhang D, Li Y. Interply friction of carbon fiber/epoxy prepreg stacks under different processing conditions. J Compos Mater 2014;48(5):515–26. https://doi.org/10.1177/0021998313476320.
- [37] Avgoulas EI, Mulvihill DM, Endruweit A, Sutcliffe MPF, Warrior NA, De Focatiis DSA, et al. Frictional behaviour of non-crimp fabrics (NCFs) in contact with a forming tool. Tribol Int 2018;121:71–7. https://doi.org/10.1016/j. triboint.2018.01.026.
- [38] Baran I, Cinar K, Ersoy N, Akkerman R, Hattel JH. A review on the mechanical modeling of composite manufacturing processes. Arch Comput Methods Eng 2017; 24:365–95. https://doi.org/10.1007/s11831-016-9167-2.
- [39] Parlevliet PP, Bersee HEN, Beukers A. Residual stresses in thermoplastic composites – a study of the literature. Part III: effects of thermal residual stresses. Compos Appl Sci Manuf 2007;38:1581–96. https://doi.org/10.1016/j. compositesa.2006.12.005.
- [40] Schneider CA, Rasband WS, Eliceiri KW. NIH Image to ImageJ: 25 years of image analysis. Nat Methods 2012;9:671–5. https://doi.org/10.1038/nmeth.2089.
- [41] Zack GW, Rogers WE, Latt SA. Automatic measurement of sister chromatid exchange frequency. J Histochem Cytochem 1977;25:741–53. https://doi.org/ 10.1177/25.7.70454.
- [42] Ridler TW, Calvard S. Picture thresholding using an iterative selection method. IEEE Transact Sys Man Cybernetics 1978;8:630–2. https://doi.org/10.1109/ TSMC.1978.4310039.
- [43] Bowden FP, Tabor D. Friction: an introduction to tribology. RE Krieger Publishing Company; 1973.
- [44] Johnson KL, Kendall K, Roberts aAD. Surface energy and the contact of elastic solids. Proc Royal Soc London A Mathematical Phys Sci 1971;324:301–13.
- [45] Hertz H. In: Lenard P, editor. Miscellaneous papers. London: Macmillan; 1896.
- [46] Blau PJ. Amontons' laws of friction. In: Wang QJ, Chung Y-W, editors. Encyclopedia of Tribology. Boston, MA: Springer US; 2013. p. 71. https://doi.org/ 10.1007/978-0-387-92897-5 166. 71.
- [47] Sahli R, Pallares G, Ducottet C, Ali IEB, Akhrass SA, Guibert M, et al. Evolution of real contact area under shear and the value of static friction of soft materials. Proc Natl Acad Sci Unit States Am 2018;115:471–6. https://doi.org/10.1073/ pngs.1706434115
- [48] Homola AM, Israelachvili JN, McGuiggan PM, Gee ML. Fundamental experimental studies in tribology: the transition from "interfacial" friction of undamaged molecularly smooth surfaces to "normal" friction with wear. Wear 1990;136: 65–83. https://doi.org/10.1016/0043-1648(90)90072-I.
- [49] Bowden FP, Bowden FP, Tabor D. The friction and lubrication of solids I. Oxford: Clarendon Press; 1950.
- [50] Dieterich JH, Kilgore BD. Direct observation of frictional contacts: new insights for state-dependent properties. Pure Appl Geophys 1994;143:283–302.
- [51] Rubinstein SM, Cohen G, Fineberg J. Contact area measurements reveal loadinghistory dependence of static friction. Phys Rev Lett 2006;96:256103. https://doi. org/10.1103/PhysRevLett.96.256103.
- [52] Creton C, Leibler L. How does tack depend on time of contact and contact pressure? J Polym Sci B Polym Phys 1996;34:545–54.
- [53] Peykova Y, Lebedeva OV, Diethert A, Müller-Buschbaum P, Willenbacher N. Adhesive properties of acrylate copolymers: effect of the nature of the substrate and copolymer functionality. Int J Adhesion Adhes 2012;34:107–16.
- [54] Tsukatani T, Hatano Y, Mizumachi H. Bonding and debonding processes in tack of pressure-sensitive adhesives. J Adhes 1989;31:59–71.

- [55] Weber B, Suhina T, Junge T, Pastewka L, Brouwer AM, Bonn D. Molecular probes reveal deviations from Amontons' law in multi-asperity frictional contacts. Nat Commun 2018;9:1–7. https://doi.org/10.1038/s41467-018-02981-y.
- [56] Ovcharenko A, Halperin G, Etsion I. In situ and real-time optical investigation of junction growth in spherical elastic-plastic contact. Wear 2008;264:1043–50. https://doi.org/10.1016/j.wear.2007.08.009.
- [57] Krick BA, Vail JR, Persson BNJ, Sawyer WG. Optical in situ micro tribometer for analysis of real contact area for contact mechanics, adhesion, and sliding experiments. Tribol Lett 2012;45:185–94. https://doi.org/10.1007/s11249-011-9870-v.
- [58] Lima M, Vasconcelos R, Abreu MJAM, Silva ME. Comparative study of friction coefficient in nonwovens using FrictorQ, Fabric Friction Tester. In: Proceedings of the 6th AUTEX 2006 Conference; 2006. Raleigh, NC.
- [59] Astrom BT. Manufacturing of polymer composites. CRC press; 1997.
- [60] Persson BN. Sliding friction: physical principles and applications. Springer Science & Business Media; 2013.
- [61] Dubois O, Le Cam J-B, Béakou A. Experimental analysis of prepreg tack. Exp Mech 2010;50:599–606. https://doi.org/10.1007/s11340-009-9236-7.
- [62] Martin CJ, Seferis JC, Wilhelm MA. Frictional resistance of thermoset prepregs and its influence on honeycomb composite processing. Compos Appl Sci Manuf 1996; 27:943–51.
- [63] Hutchings I, Shipway P. Tribology: friction and wear of engineering materials. Ann Arbor, MI: Butterworth-Heinemann; 2017.
- [64] Ramkumar SS, Umrani AS, Shelly DC, Tock RW, Parameswaran S, Smith ML. Study of the effect of sliding velocity on the frictional properties of nonwoven fabric substrates. Wear 2004;256:221–5. https://doi.org/10.1016/S0043-1648(03) 00440-X.
- [65] Kim J-Y, Hwang Y-T, Baek J-H, Song W-Y, Kim H-S. Study on inter-ply friction between woven and unidirectional prepregs and its effect on the composite forming process. Compos Struct 2021;267:113888. https://doi.org/10.1016/j. compstruct.2021.113888.
- [66] Ruina A. Slip instability and state variable friction laws. J Geophys Res Solid Earth 1983;88:10359–70. https://doi.org/10.1029/JB088iB12p10359.
- [67] Hulikal S, Lapusta N, Bhattacharya K. Static and sliding contact of rough surfaces: effect of asperity-scale properties and long-range elastic interactions. J Mech Phys Solid 2018;116:217–38. https://doi.org/10.1016/j.jmps.2018.03.022.
- [68] Aharonov E, Scholz CH. A physics-based rock friction constitutive law: steady state friction. J Geophys Res Solid Earth 2018;123:1591–614. https://doi.org/10.1002/ 2016.JB013829.
- [69] Rice JR, Lapusta N, Ranjith K. Rate and state dependent friction and the stability of sliding between elastically deformable solids. J Mech Phys Solid 2001;49:1865–98. https://doi.org/10.1016/S0022-5096(01)00042-4.
- [70] Gillanders AM, Kerr S, Martin TJ. Determination of prepreg tack. Int J Adhesion Adhes 1981;1:125–34. https://doi.org/10.1016/0143-7496(81)90035-X.
- [71] Budelmann D, Detampel H, Schmidt C, Meiners D. Interaction of process parameters and material properties with regard to prepreg tack in automated layup and draping processes. Compos Appl Sci Manuf 2019;117:308–16. https://doi. org/10.1016/j.compositesa.2018.12.001.
- [72] Hamrock BJ, Schmid BJ, Jacobson BO. Fundamentals of fluid film lubrication. CRC Press; 2004.
- [73] Larberg YR, Åkermo M. On the interply friction of different generations of carbon/epoxy prepreg systems. Compos Appl Sci Manuf 2011;42:1067–74. https://doi.org/10.1016/j.compositesa.2011.04.010.
- [74] Kalebek NA, Babaarslan O. Effect of weight and apllied force on the friction coefficient of the spunlace nonwoven fabrics. Fibers Polym 2010;11:277–84. https://doi.org/10.1007/s12221-010-0277-4.
- [75] Ibrahem RA. Friction and wear behaviour of fibre/particles reinforced polyester composites. Int J Appl Math Res 2016;2:22–6.
- [76] Blau PJ. Scale effects in sliding friction: an experimental study. In: Singer IL, Pollock HM, editors. Fundamentals of friction: macroscopic and microscopic processes. Dordrecht: Springer Netherlands; 1992. p. 523–34. https://doi.org/ 10.1007/978-94-011-2811-7 26.
- [77] Dowson D, Priest M, Taylor CM, Ehret P, Childs THC, Dalmaz G, et al. Thinning films and tribological interfaces: proceedings of the 26th leeds-lyon symposium. Elsevier; 2000.
- [78] Müser MH, Dapp WB, Bugnicourt R, Sainsot P, Lesaffre N, Lubrecht TA, et al. Meeting the contact-mechanics challenge. Tribol Lett 2017;65:118. https://doi. org/10.1007/s11249-017-0900-2.
- [79] Malekan A, Rouhani S. Model of contact friction based on extreme value statistics. Friction 2019;7:327–39. https://doi.org/10.1007/s40544-018-0215-9.
- [80] Baumberger T, Berthoud P, Caroli C. Physical analysis of the state- and rate-dependent friction law. II. Dynamic friction. Phys Rev B 1999;60:3928–39. https://doi.org/10.1103/PhysRevB.60.3928.
- [81] Bureau L, Baumberger T, Caroli C. Rheological aging and rejuvenation in solid friction contacts. Eur Phys J E 2002;8:331–7. https://doi.org/10.1140/epje/i2002-10017-1.
- [82] Crossley RJ, Schubel PJ, De Focatiis DSA. Time-temperature equivalence in the tack and dynamic stiffness of polymer prepreg and its application to automated composites manufacturing. Compos Appl Sci Manuf 2013;52:126–33. https://doi. org/10.1016/j.compositesa.2013.05.002.
- [83] Smith AW, Endruweit A, Choong GYH, De Focatiis DSA, Hubert P. Adaptation of material deposition parameters to account for out-time effects on prepreg tack. Compos Appl Sci Manuf 2020;133:105835. https://doi.org/10.1016/j. compositesa.2020.105835.